

Subnanokelvin thermometry of an interacting d -dimensional homogeneous Bose gas

Muhammad Miskeen Khan,^{1,2,3,4} Mohammad Mehboudi ,^{5,2} Hugo Terças,^{1,3} Maciej Lewenstein ,^{2,6}
and Miguel Angel Garcia-March ^{2,7}

¹*Instituto Superior Técnico, Universidade de Lisboa, Portugal*

²*ICFO – Institut de Ciències Fotòniques, The Barcelona Institute of Science and Technology,
Av. Carl Friedrich Gauss 3, 08860 Castelldefels (Barcelona), Spain*

³*Instituto de Plasmas e Fusão Nuclear, Instituto Superior Técnico, Universidade de Lisboa, Portugal*

⁴*JILA, National Institute of Standards and Technology and University of Colorado, 440 UCB, Boulder, Colorado 80309, USA*

⁵*Département de Physique Appliquée, Université de Genève, CH-1211 Genève, Switzerland*

⁶*ICREA, Pg. Lluís Companys 23, 08010 Barcelona, Spain*

⁷*Instituto Universitario de Matemática Pura y Aplicada, Universitat Politècnica de València, E-46022 València, Spain*



(Received 17 September 2021; revised 17 January 2022; accepted 7 March 2022; published 6 June 2022)

We propose experimentally feasible means for nondestructive thermometry of *homogeneous* Bose-Einstein condensates in different spatial dimensions ($d \in \{1, 2, 3\}$). Our impurity-based protocol suggests that the fundamental error bound on thermometry at the subnanokelvin domain depends highly on the dimension, in that the higher the dimension the better the precision. Furthermore, suboptimal thermometry of the condensates by using measurements that are experimentally feasible is explored. We specifically focus on measuring position and momentum of the impurity that belong to the family of Gaussian measurements. We show that, generally, experimentally feasible measurements are far from optimal, except in one dimension, where position measurements are indeed optimal. This makes realistic experiments perform very well at few nanokelvin temperatures for all dimensions, and at subnanokelvin temperatures in the one-dimensional scenario. These results take a significant step towards experimental realization of probe-based quantum thermometry of Bose-Einstein condensates, as it deals with them in one, two, and three dimensions and uses feasible measurements applicable in current experimental setups.

DOI: [10.1103/PhysRevResearch.4.023191](https://doi.org/10.1103/PhysRevResearch.4.023191)

I. INTRODUCTION

The fundamental and technological importance of temperature of quantum systems has led to the rapid development of the theory of *quantum thermometry* [1,2]. Among the fundamental questions of interest in this subject are (i) what are the ultimate limits on thermometry precision? and (ii) what is the best measurement?—which is mainly relevant for quantum systems due to the *incompatibility* of measurements. Often, quantum thermometry proposals are probe based, in that, the information about the unknown temperature of a sample is registered on the quantum state of a probe (thermometer) through some sort of *sample-probe* interaction [3–5]. By performing a suitable measurement on the probe, one aims to infer the temperature with minimal *statistical error*. This forms a nondestructive thermometry strategy, thanks to the fact that the probe size is significantly smaller than the sample, and that the sample is not directly measured. The theory of probe-based thermometry has been adapted to describe various platforms such as fermionic or bosonic samples, and by using different resources like entanglement, criticality, and

coherence [3–20]. When probes equilibrate with the sample the answer to (i) is given by the heat capacity of the probe, and as for (ii), energy measurements are the most precise ones [6]. Nonetheless, we know from the theory of open quantum systems that probes rarely thermalize with the sample that they interact with [21,22]. This phenomena is specifically relevant at low temperatures and/or strong probe-sample coupling. Therefore, the impact of nonthermalizing probes in thermometry, specifically of bosonic gases, has been considered in several works. For example, it is shown that depending on the temperature regime, strong probe-sample interaction can be beneficial or disadvantageous for thermometry [3,23]. The extremely determinant role of spectral density at low temperature thermometry was considered in [10], and the impact of bath induced correlations present at low temperatures were addressed in [24]. This work is dedicated to thermometry of *homogeneous* or uniform ultracold Bosonic gases, in *any spacial dimensionality*. We provide answers to the fundamental questions (i) and (ii) for *local* thermometry settings and address the practical problem of (iii) designing experimentally feasible measurements that perform fairly close to optimal.

Homogeneous ultracold gases represent a unique platform to test fundamental quantum phenomena, and have a high potential for quantum technologies. They can be realized experimentally in very versatile and extremely controlled setups. First realizations were obtained in a uniform three-dimensional (3D) optical box trap, formed by a *tube* laser beam and two perpendicular *sheet* laser beams [25] (forming

Published by the American Physical Society under the terms of the [Creative Commons Attribution 4.0 International](https://creativecommons.org/licenses/by/4.0/) license. Further distribution of this work must maintain attribution to the author(s) and the published article's title, journal citation, and DOI.

a dark optical trap, see [26,27]). This experiment allowed for a thorough characterization of the properties of the gas, such as the condensate interaction energy [28], or the critical point for condensation [29]. A similar technique was used in [30] to realize uniform Bose gases in a two-dimensional (2D) boxlike potential, which is confined in an annular geometry contained between an external ring and an inner disk. Uniform ultracold Bose gases in a variety of two-dimensional configurations (e.g., disk, rectangle, double rectangle), were further explored in [31]. The establishment of this neat experimental tool paved the way to study a large collection of fundamental phenomena in uniform gases, e.g., supercurrents [30], the Kibble-Zurek mechanism [30–33], the power-law scaling of the coherence length [32], the quantum version of the Joule-Thomson effect [29], several aspects of the depletion and quasiparticle excitations [34,35], or giant vortex clusters, recently [36].

Experiments in uniform Bose-Einstein condensates have thus shown that they are outstandingly controllable systems which allow us to test many fundamental effects. On top of this, there is a large number of theoretical proposals which take advantage of their properties for which the uniformity of the gas and the associated universality of the long-wave behavior is crucial. Moreover, the great uniformity of this system makes it a great setup for correlation studies for very low temperatures ($T \rightarrow 0$ see [28]). To date, most theoretical works in thermometry of cold gases have fallen short in being applied to experiments, first, because the theory involves oversimplifications as they consider toy models as a proof of concept. Second, due to technological limitations the thermometry schemes with ultimate precision are not experimentally feasible. Nonetheless, probe-based thermometry of ultracold gases with suboptimal precision have been experimentally realized in particular cases [37].

Our proposal is therefore of large interest in studies of uniform BECs due to its nondestructive feature, rigorous modeling, and high precision with experimentally realizable measurements. Such temperature estimation will boost, e.g., characterization of phase diagrams [38–44], or help to account for thermal fluctuations and separate them from the quantum ones. Furthermore, this thermometer keeps its accuracy at very low temperatures, a regime in which the uniform gases promise a large number of interesting effects and applications (e.g., this system has been proposed as a quantum simulator of the early universe [45–47] or for relativistic quantum metrology, as acceleration produces observable relativistic effects on homogeneous BECs [48]). Particularly, our first-of-its-kind exploration of impurity-based thermometry in one-, two-, and three-dimensional homogeneous Bosonic gases suggest that the ultimate precision substantially improves by increasing the spatial dimension, and thus giving more importance to the thermal fluctuations in 3D Bosonic gases. As an example, one can estimate the subnanokelvin temperature of a 3D Bosonic gas in a homogeneous trap with a relative error below 13% with as few as 100 measurement runs, whereas in the one-dimensional (1D) scenario one needs more than 500 measurements for the same precision. We further explore more practical measurements, namely based on the position and momentum of the impurity. Indeed, they can perform well compared to the ultimate bound: For the same target precision they may need twice as many measurements as the optimal (but experimentally complex) measurement. For

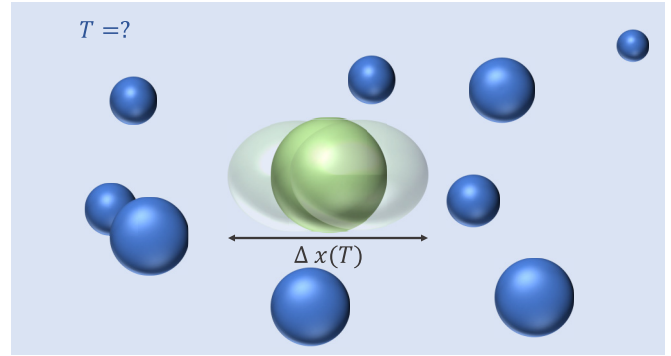


FIG. 1. Schematic of our proposed thermometry protocol. The sample is a collection of BEC atoms (represented by the blue balls) trapped in a uniform potential/box with arbitrary dimension $d \in \{1, 2, 3\}$. An impurity atom (represented by the green ball) plays the role of our thermometer. The impurity is trapped in a harmonic potential (not shown here). After allowing for sufficiently long interaction, the quantum state of the impurity atom acquires information about the temperature T of the sample. By measuring some property of the impurity, e.g., its position fluctuations, one can infer T by minimally disturbing the BEC sample.

the 1D scenario and at low enough temperatures the position measurement is *de facto* optimal.

II. IMPURITY DYNAMICS IN A BEC

Our setup is illustrated in Fig. 1. We consider an impurity atom with mass m_I in an external potential $U_{\text{ext}}(\mathbf{r})$. The impurity atom is immersed within a hosting BEC. We consider a homogeneous BEC of dimension d . In total, the Hamiltonian describing the noninteracting parts and all the interactions of such a composite system is given by

$$H = H_I + H_B + H_{BB} + H_{IB}. \quad (1)$$

Here the four terms represent the noninteracting Hamiltonians of the impurity and of the bosons, and the Hamiltonians of the boson-boson atomic interaction and the impurity-boson atomic interaction, respectively. Within the second quantization formalism, their explicit forms are [49]

$$H_I = \frac{\mathbf{p}^2}{2m_I} + U_{\text{ext}}(\mathbf{r}), \quad H_B = \sum_{\mathbf{k}} \epsilon_{\mathbf{k}} a_{\mathbf{k}}^\dagger a_{\mathbf{k}}, \quad (2)$$

$$H_{BB} = \frac{1}{2V} \sum_{\mathbf{k}, \mathbf{k}', \mathbf{q}} V_B(\mathbf{q}) a_{\mathbf{k}'-\mathbf{q}}^\dagger a_{\mathbf{k}+\mathbf{q}}^\dagger a_{\mathbf{k}'} a_{\mathbf{k}}, \quad (3)$$

$$H_{IB} = \frac{1}{V} \sum_{\mathbf{k}, \mathbf{q}} V_{IB}(\mathbf{q}) a_{\mathbf{k}-\mathbf{q}}^\dagger a_{\mathbf{k}}. \quad (4)$$

In $d < 3$, the external potential experienced by the bosons, $V_{\text{ext}}(\mathbf{r})$, and that of the impurity, $U_{\text{ext}}(\mathbf{r})$, are tightly parabolic in the directions in which the degrees of freedom of the BEC and the impurity are frozen, so to realize the reduction of dimensionality. In $d = 3$, and for $d < 3$ in all directions where dimensionality is not reduced, the external potential for the bosons is zero and the potential for the impurity $U_{\text{ext}}(\mathbf{r})$ is parabolic with trapping frequency Ω . Then, in these directions, the BEC is homogeneous and contained in spatial domain of size V , say a uniform box in $d = 3$ [32], a quasi-2D

uniform potential [31], or even an annulus geometry [30]. The bosonic operators $a_{\mathbf{k}}$ ($a_{\mathbf{k}}^\dagger$) destroy (create) a boson of mass m_B having wave vector \mathbf{k} and energy $\epsilon_{\mathbf{k}}$. The quantities V_B and V_{IB} represent the Fourier transforms of the impulsive (contact) boson-boson and impurity-boson interactions, respectively. In addition, the impurity density in the momentum space is $\rho_1(\mathbf{q})$. The Hamiltonian can be recast in the form of a Fröhlich Hamiltonian, with some constraints over the values of the parameters of the system (like the temperature, trapping frequency Ω for the impurity, or strength of interactions, see Appendix C in [49] and for the trapped case and higher dimensions see [50,51]). We call the regime in which all these conditions are fulfilled the Fröhlich regime, and we check in all the calculations presented in this paper that indeed these conditions are fulfilled. Then, in this regime, the Hamiltonian can be written as

$$H = \frac{\mathbf{P}^2}{2m_1} + U_{\text{ext}}(\mathbf{r}) + \sum_{\mathbf{k} \neq 0} E_{\mathbf{k}} b_{\mathbf{k}}^\dagger b_{\mathbf{k}} + \sum_{\mathbf{k} \neq 0} \hbar \mathbf{g}_{\mathbf{k}} \cdot \mathbf{r} \pi_{\mathbf{k}}. \quad (5)$$

In Eq. (5) the first term represents the free kinetic energy of the impurity. The last term is the interaction between the position coordinate \mathbf{r} of the impurity atom and the Bogoliubov bosonic modes of BEC. This interaction part is linear when the constraints over the parameters mentioned above are fulfilled [49,51]. This part of the Hamiltonian is written in terms of its canonical dimensionless momenta $\pi_{\mathbf{k}} = i(b_{\mathbf{k}} - b_{\mathbf{k}}^\dagger)$, with $b_{\mathbf{k}}$ ($b_{\mathbf{k}}^\dagger$) representing the Bogoliubov annihilation (creation) operator for the mode with momentum \mathbf{k} . It thus has the form of the quantum Brownian motion (QBM) model, in which the impurity plays the role of a Brownian particle, while the Bogoliubov modes of BEC act as an effective bosonic environment. Such an environment forms the multimode thermal states due to the finite temperature of the gas. The coupling constant is given by

$$\mathbf{g}_{\mathbf{k}} = \frac{\mathbf{k} V_{\mathbf{k}}}{\hbar}, \quad V_{\mathbf{k}} = g_{IB} \sqrt{\frac{n_0}{V}} \left[\frac{(\xi |\mathbf{k}|)^2}{(\xi |\mathbf{k}|)^2 + 2} \right]^{1/4}. \quad (6)$$

In the above expressions, the coherence length and the speed of sound are, respectively, given as

$$\xi = \frac{\hbar}{\sqrt{2g_B m_B n_0}}, \quad c = \frac{\hbar}{\sqrt{2m_B \xi}}. \quad (7)$$

Within the linear Bogoliubov dispersion relation, it has been shown that the bath is conveniently described by the superohmic spectral density tensor $\underline{J}_d(\omega) = d^{-1} [\mathcal{J}_d(\omega)]_{d \times d}$ for the dimension d of the hosting BEC (see Appendix C and Ref. [51] for further details). In this expression, the spectral function \mathcal{J}_d is shown to take the superohmic form

$$\mathcal{J}_d(\omega) = m_1 (\tau_d)^d \omega^{d+2} \mathcal{K}(\omega, \Lambda_d), \quad (8)$$

while we introduce the sharp ultraviolet cut-off \mathcal{K} with a cut-off frequency Λ_d . This is customary to avoid divergences due to the rising behavior of the spectral density at high frequencies. Here the d -parametrized characteristic time τ_d is given by

$$(\tau_d)^d = \frac{S_d (\eta_d)^2}{2(2\pi)^d m_1} \left(\frac{m_B}{[g_{B,d}]_{[\frac{d}{d+2}]} n_{0,d}} \right)^{\frac{(d+2)}{2}}. \quad (9)$$

For $d = 1, 2$, and 3 we have $S_1 = 2$, $S_2 = 2\pi$, and $S_3 = 4\pi$, respectively, while the d -parametrized bath characteristic frequency is $\Lambda_d = (g_{B,d} n_{0,d})/\hbar$. We have additionally written the impurity-Boson coupling in the units of the boson-boson coupling as $\eta_d = (g_{IB,d}/g_{B,d})$. In addition, the d -dimensional density is $n_{0,d} = (n_{0,1})^d$. The external potential for the BEC atoms, which contains the transverse harmonic confinement of BEC for $d < 3$ that realizes the reduction of dimensionality, is explicitly given by

$$V_{\text{ext}}(\mathbf{r}) = \begin{cases} (1/2)m_B \omega_1^2 (y^2 + z^2), & \text{for } d = 1, \\ (1/2)m_B \omega_z^2 (z^2), & \text{for } d = 2, \\ 0, & \text{for } d = 3. \end{cases} \quad (10)$$

The boson-boson coupling $g_{B,d}$ is written in terms of the external trap frequency $\omega_d = \{\omega_1 = \omega_\perp, \omega_2 = \omega_z, \omega_3 = 0\}$ for the dimension involved, and it has the expression [52,53]

$$g_{B,d} = \frac{S_d \hbar^2 a_3}{m_B (\sqrt{\hbar/m_B \omega_d})^{3-d}}. \quad (11)$$

This makes the cases $d = 1$ and $d = 2$ to be quasi-1D and quasi-2D, respectively. In Ref. [51], the above bath characterization has been employed to derive the equations of motion (EOM) of the impurity position coordinates, while taking into account the bath memory effects. This is accounted for by the time-nonlocal form of the damping kernel with its tensor component Γ_d^{xx} , and x in one of the relevant directions (in $d = 2$ and $d = 3$ similar expressions are found in the other directions). The harmonically bound impurity motion is driven by the effective Brownian stochastic force $B^x(t)$, which is further formed by the Bogoliubov modes of the BEC. The corresponding EOM reads

$$\ddot{x}(t) + \Omega^2 x(t) + \partial_t \int_0^t \Gamma_d^{xx}(t-s)x(s)ds = \left(\frac{1}{m_1} \right) B^x(t), \quad (12)$$

with x representing the position of the impurity in one of the relevant directions. The solution of this equation is shown to take form

$$x(t) = G_{1,d}(t)x(0) + G_{2,d}(t)\dot{x}(0) + (1/m_1) \int_0^t ds G_{2,d}(t-s)B^x(s), \quad (13)$$

where we formulate the Green's functions $G_{1,d}$ and $G_{2,d}$ through their Laplace transforms

$$\mathcal{L}_{S,d}[G_{1,d}(t)] = \frac{\mathcal{S}}{\mathcal{S}^2 + \Omega^2 + \mathcal{S} \mathcal{L}_{S,d}[\Gamma_d^{xx}(t)]}, \quad (14)$$

$$\mathcal{L}_{S,d}[G_{2,d}(t)] = \frac{1}{\mathcal{S}^2 + \Omega^2 + \mathcal{S} \mathcal{L}_{S,d}[\Gamma_d^{xx}(t)]}. \quad (15)$$

By introducing the sharp cutoff given by $\mathcal{K} = \Theta(\Lambda_d - \omega)$, with Θ as the Heaviside step function, the d -parametrized damping kernel reads

$$\mathcal{L}_{S,d}[\Gamma_d^{xx}(t)] = \frac{(\Lambda_d)^{d+2} (\tau_d)^d {}_2F_1\left(1, \frac{d+2}{2}, \frac{d+4}{2}; -\frac{(\Lambda_d)^2}{\mathcal{S}^2}\right)}{d(d+2)\mathcal{S}}, \quad (16)$$

with ${}_2F_1[\cdot]$ denoting the hypergeometric function.

In the following we aim to use the impurity motion statistical properties to estimate the temperature of the BEC, generalizing to any dimension and homogeneous gases the proposal introduced in [3] for one-dimensional and trapped gases. The quadratures of interest are the position and momentum of the impurity. Additionally, the Gaussian nature of its dynamics is fully characterized by its covariance matrix. In order to quantify the dynamics of the impurity, we start by writing a formal representation of the steady state covariance matrix of the impurity. It is important to note that the steady state covariance matrix is diagonal taking the form $\sigma \equiv \text{diag}(\Delta x^2, \Delta p^2)$. Here Δx^2 and Δp^2 (with zero-mean values) are the steady state position and momentum variances of the impurity mechanical mode, which are appropriately scaled such that the uncertainty relation reads $\Delta x \Delta p \geq 1$ [54]. The fundamental expressions of the position and momentum variances in the unscaled coordinates has explicit connectivity to the imaginary part of the susceptibility $\tilde{\chi}_d''(\omega)$ (fluctuation-dissipation theorem), that is,

$$\langle x^2 \rangle_d = \frac{\hbar}{\pi} \int_0^\infty d\omega \coth\left(\frac{\hbar\omega}{2k_B T}\right) \tilde{\chi}_d''(\omega), \quad (17)$$

$$\langle p^2 \rangle_d = \frac{\hbar m_1^2}{\pi} \int_0^\infty d\omega \omega^2 \coth\left(\frac{\hbar\omega}{2k_B T}\right) \tilde{\chi}_d''(\omega), \quad (18)$$

where

$$\tilde{\chi}_d''(\omega) = \frac{1}{m_1} \frac{\xi_d^{xx}(\omega)\omega}{[\omega\xi_d^{xx}(\omega)]^2 + [\Omega^2 - \omega^2 + \omega\theta_d^{xx}(\omega)]^2}. \quad (19)$$

We point out that any kind of *superohmicity* (and also the dimensional information) is captured here by the functions $\xi_d^{xx}(\omega)$ and $\theta_d^{xx}(\omega)$ which are, respectively, the Fourier domain real and imaginary part of the damping kernel [cf. Eq. (16)].

III. THERMOMETRY OF BEC IN DIFFERENT DIMENSIONS

Estimation theory, in part, deals with inference of a parameter \mathcal{P} from a set of measurement outcomes with the aim of minimizing the estimation error. This set is collected through performing a positive operator-valued measurement (POVM) on the quantum system, with a density matrix $\hat{\rho}(\mathcal{P})$ that depends on the parameter. Let $\{\hat{\Pi}_x^k\}$ represent the POVM elements of the measurement. Here k denotes the choice of measurement while \mathbf{x} labels different outcomes. Then $\hat{\Pi}_x^k \geq 0$ and we have $\int d\mathbf{x} \hat{\Pi}_x^k = \mathbb{I}$, $\forall k$. The uncertainty (randomness) in the POVM outcomes allows us only to infer the parameter with limited precision. According to the Crámer-Rao bound for an unbiased estimator the estimation error—as quantified by the mean squared error and denoted by $\text{Var}(\mathcal{P}, k)$ —is lower bounded by the inverse of the Fisher information, which is $\text{Var}(\mathcal{P}, k) \geq [NF(\mathcal{P}, k)]^{-1}$. Here N is the number of (independent) measurement runs and appears as a result of the central limit theorem. The Fisher information $F(\mathcal{P}, k)$ is given by

$$F(\mathcal{P}, k) = \int [\partial_{\mathcal{P}} \ln p(\mathbf{x}|\mathcal{P}, k)]^2 p(\mathbf{x}|\mathcal{P}, k) d\mathbf{x}, \quad (20)$$

with $p(\mathbf{x}|\mathcal{P}, k) = \text{Tr}[\hat{\rho}(\mathcal{P})\hat{\Pi}_x^k]$ being the distribution of the measurement outcomes, conditioned on the true value of the

parameter to be \mathcal{P} and the measurement k being performed. Note that the Cramér-Rao bound can be saturated using the maximum likelihood estimator.

The Fisher information clearly depends on the specific measurement performed, hence the argument k . One may optimize it over all possible measurements to get the so called quantum Fisher information (QFI) that quantifies yet another fundamental lower bound on the estimation error regardless of the measurement. The QFI can be written as [55,56]

$$F^Q(\mathcal{P}) := \max_k F(\mathcal{P}, k) = \text{Tr}[\hat{\rho}(\mathcal{P})\hat{\Lambda}^2(\mathcal{P})], \quad (21)$$

where the Hermitian operator $\hat{\Lambda}(\mathcal{P})$ is the symmetric logarithmic derivative (SLD) defined as

$$\partial_{\mathcal{P}} \hat{\rho}(\mathcal{P}) \equiv \{\hat{\Lambda}(\mathcal{P}), \hat{\rho}(\mathcal{P})\}/2. \quad (22)$$

In fact, a measurement performed in the basis of SLD is optimal.

Generally speaking, finding the optimal measurement and/or the ultimate error bound is a challenging task. Nonetheless, as we proved in the previous section, here we are dealing with a bosonic Gaussian system, which is fully characterized by its displacement vector and covariance matrix. It has been shown that the QFI of Gaussian systems can be written in terms of the covariance matrix σ , as follows [57–60]:

$$F^Q(\mathcal{P}) = \frac{1}{2} \frac{\text{Tr}[(\sigma^{-1}[\partial_{\mathcal{P}}\sigma])^2]}{1 + \mu^2} + 2 \frac{(\partial_{\mathcal{P}}\mu)^2}{1 - \mu^4}. \quad (23)$$

Here $\mu = 1/\sqrt{\Delta x^2 \Delta p^2}$ is the purity function of the impurity state. The optimal measurement that achieves the QFI can be also found analytically. For our thermometry problem we have $\mathcal{P} = T$, and use Eqs. (17) and (18) to obtain the optimal measurement. This is generally a projective measurement in the basis of $\hat{\Lambda}(T) \equiv C_x(T)(\hat{x}^2 - \langle \hat{x}^2 \rangle) + C_p(T)(\hat{p}^2 - \langle \hat{p}^2 \rangle)$, where the coefficients $C_p(T)$ and $C_x(T)$ are temperature dependent [57,61]. While measuring position and momentum are experimentally feasible via *time-of-flight* or *in situ* absorption imaging, unfortunately performing the optimal measurement is often not practical since it involves both \hat{x}^2 and \hat{p}^2 .

For any measurement we let our figure of merit to be $\delta T(k)/T := \sqrt{NT^2 F(T, k)}$ which is the relative temperature error using the measurement k and maximum likelihood estimator; the smaller it is, the more precise the thermometer will be. One has $\delta T(k)/T \geq \sqrt{NT^2 F^Q(T)} = \delta T(\hat{\Lambda})/T := \delta T_{\min}/T$. In what follows we examine the optimal and experimentally feasible suboptimal measurements in different spacial dimensions.

A. The optimal thermometry and the fundamental bounds

In Fig. 2 we fix the temperature, and show the relative temperature error $\delta T_{\min}/T$ versus the dimensionless system-bath coupling η . The relative error peaks at some coupling $\eta_{p,d}$ that depends on the temperature and the dimensionality. For the regime where $\eta < \eta_{p,d}$, the error increases as we strengthen the system-bath coupling. On the other hand, for $\eta > \eta_{p,d}$, the opposite is observed. For the latter case, however, the enhancement of the coupling is limited by the maximum allowed

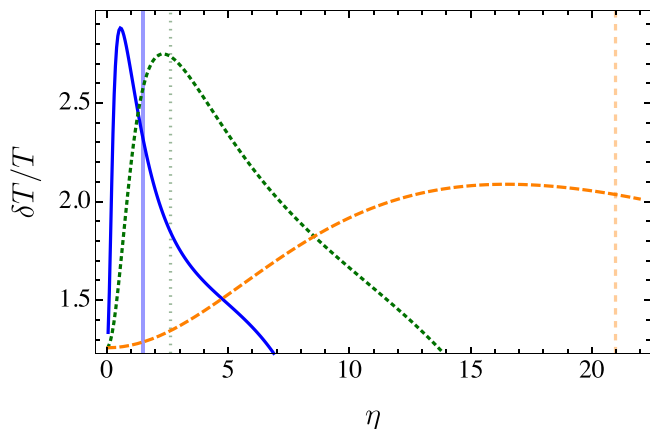


FIG. 2. Minimum relative temperature error—obtained by measuring $\hat{\Lambda}$ —as a function of the dimensionless system-bath coupling. Solid blue, dotted green, and dashed orange curves represent the 1D, 2D, and 3D cases, respectively. The corresponding background vertical lines set the upper bound of the coupling $\eta_{c,d}$ for the validity of the Fröhlich regime. The three-dimensional scattering length is $a_3 = 100a_0$. The 1D density is kept to be $n_{0,1} = 3 (\mu\text{m})^{-1}$. For the cases of quasi-1D and 2D settings, we have set bosons transverse confinement frequency to be $\omega_{\perp} = \omega_z = 2\pi \times 34$ kHz. These results correspond to $T = 0.2$ nK for all the dimensions. The impurity trapping frequency is $\Omega = 2\pi \times 10$ Hz. The number of measurements are $N = 1$. These results refers to a potassium K impurity atom with mass $m_I = 6.4924249 \times 10^{-26}$ kg, immersed in a gas of rubidium Rb atoms with mass $m_B = 1.44316060 \times 10^{-25}$ kg.

system-bath coupling $\eta_{c,d}$ in order to keep the calculations within the Fröhlich regime (see caption of Fig. 2). As shown in Appendix A, for all the dimensions, the thermal statistics of the impurity is mostly contributed by the ground state for $\eta < \eta_{p,d}$. Such regime would then reflect a state with high purity. For the case of $\eta > \eta_{p,d}$ higher order Fock states significantly contribute in the construction of such statistics and the state becomes more mixed. This leads to the results that smaller values of the coupling—as characterized by $\eta < \eta_{p,d}$ —are suitable for thermometry only as long as the system closely follows the ground state with high purity. Yet, for a strongly coupled bath with the system ($\eta > \eta_{p,d}$)—where bath induced thermalization occurs—the large coupling values give better thermometric performance. However, the latter regime is always bounded above by some critical coupling in the present physical setup. Finally, from Fig. 2, the peak error is relatively reduced as we move to higher dimensions reflecting that higher dimensions are better for thermometry. In order to further analyze the performance of the thermometer, we plot the relative temperature error versus the true temperature of the hosting BEC for different dimensions in Fig. 3. For temperature range of interest— $0.2 \leq T \leq 10$ nK—higher d always leads to smaller error. This is an evidence that for high enough temperatures larger nonohmicity (which is related to higher dimension) leads to better thermometry precision. In [23], a similar behavior is reported. There it is also shown that at extremely low temperatures, the opposite behavior is observed, i.e., lower nonohmicity leads to higher precision. Nonetheless, for our BEC setup such extreme lows are irrelevant as they fall even below the picokelvin regime. For $d = 3$

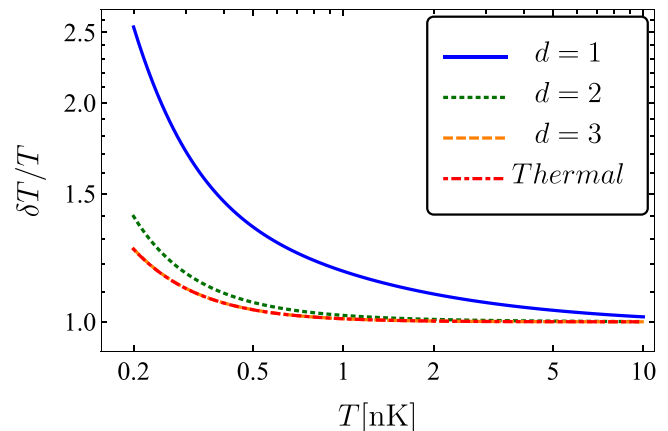


FIG. 3. Minimum relative temperature error as a function of the temperature. We set the coupling to $\eta = 0.3$. For comparison we also plot the error of a thermal state, which matches the $d = 3$ case for the range of temperatures considered here. The rest of the parameters are the same as in Fig. 2.

scenario we observe that the $\delta T_{\min}/T \simeq 1.25$ at $T = 0.2$ nK for a single shot. Thus with $N = 100$ measurements one gets a relative error of $\simeq 12.5\%$. In $d = 1$ the same precision requires about $N = 400$ measurements. For temperatures $T \gtrsim 1$ nK the relative error in two and three dimensions saturate to $\delta T_{\min}/T \simeq 1$, i.e., one can have 10% error with $N = 100$ measurements. This is in fact a result that one expects when the impurity is thermalized and the ratio $T/\Omega \gg 1$. For the one-dimensional scenario, the saturation of error only appears for $T \gtrsim 10$ nK. We also show the relative error down to 50 pK in Appendix B, serving as a guide to the eye about the error enhancement at low temperature.

B. Suboptimal thermometry and feasible measurements

Now that we have found the ultimate precision bounds on estimating the temperature of the BEC, we move forward to examine the estimation error by measuring more practical observables, namely an individual measurements of either on position or momentum of the impurity [62].

We note that both position and momentum belong to the family of Gaussian measurements, and can be fully characterized by an associated covariance matrix σ^k , with $k \in \{\hat{x}, \hat{p}\}$ labeling the measurement. In particular, we have $\sigma^{\hat{x}} = \lim_{R \rightarrow \infty} \text{diag}(1/R, R)$, and $\sigma^{\hat{p}} = \lim_{R \rightarrow \infty} \text{diag}(R, 1/R)$, with R being some squeezing parameter. When performed on a system with covariance matrix σ , the corresponding Fisher information of these measurements is given by [61]

$$F(T, k) = \frac{1}{2} \text{Tr}\{[(\sigma^k + \sigma)^{-1} \partial_T (\sigma^k + \sigma)]^2\}. \quad (24)$$

By doing some algebra we find

$$F(T, \hat{x}) = \frac{|\partial_T \langle \hat{x}^2 \rangle|^2}{2 \langle \hat{x}^2 \rangle^2} = \frac{|\partial_T \langle \hat{x}^2 \rangle|^2}{\text{Var}(\hat{x}^2)}, \quad (25)$$

which is nothing but the (inverse) of error propagation for the observable \hat{x}^2 . A similar relation connecting the Fisher information of measuring \hat{p} and the error propagation of the observable \hat{p}^2 holds by changing $\hat{x} \rightarrow \hat{p}$.

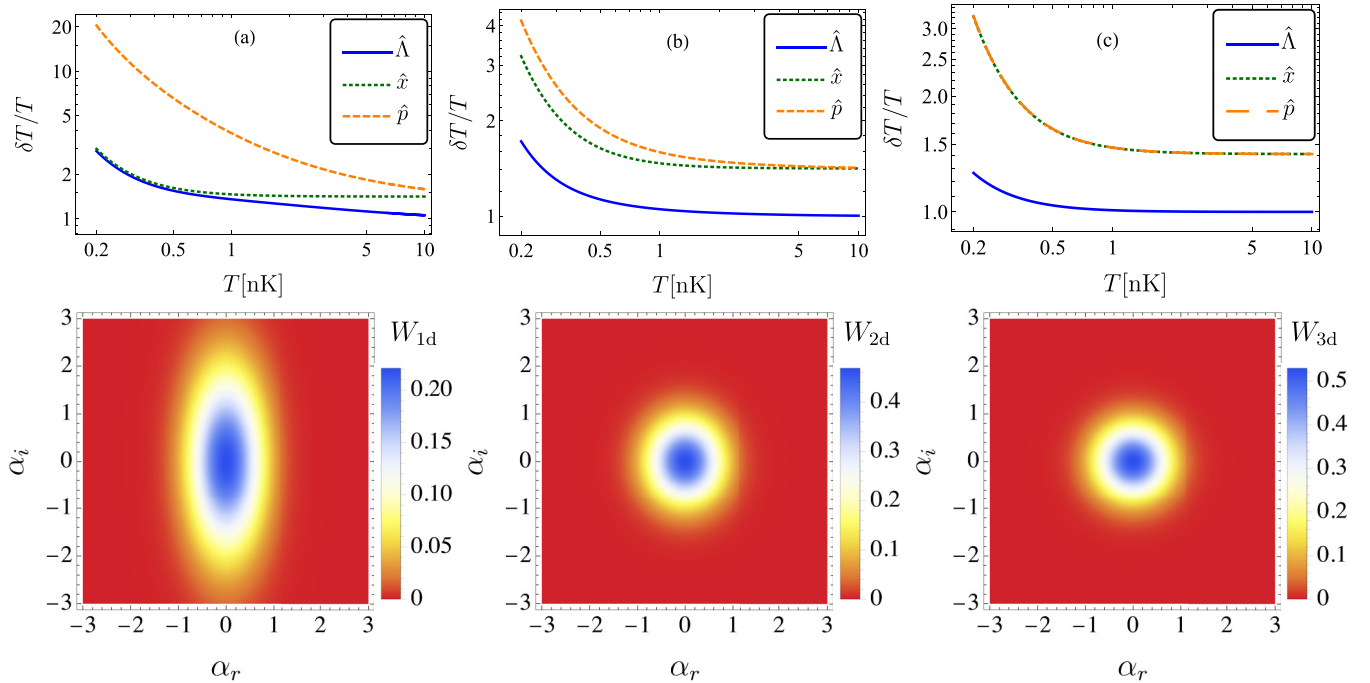


FIG. 4. Upper panels: Relative error as a function of coupling based on quadrature measurements (\hat{x} and \hat{p}) as well as the optimal measurement $\hat{\Lambda}$. (a), (b), and (c) The 1D, 2D, and 3D cases, respectively. For all plots we set $\eta = 0.6$ and $N = 1$. Lower panels: Corresponding to each case above, the Wigner function of the impurity state is plotted against the phase space variables α_r and α_i and for $T = 0.2$ nK. In the 1D case, an enhanced position squeezing is obtained, while as we move to higher dimensions, we obtain a lesser position squeezing effect.

In Figs. 4(a)–4(c) we depict, for all dimensions, the relative temperature error by measuring position and momentum and compare them to the optimal—yet challenging—measurement. Quite notably, in the quasi-1D setting, the position-based measurement reaches the optimal profile in the low temperature regime, i.e., below $T \lesssim 1$ nK. This is because of the notable position squeezed states of the impurity motion in the 1D case. As such, the Fisher information scales as $F(T, \hat{x}) \sim 1/\Delta x^4$. Therefore, the small amount of noise in the position would lead to an enhanced value of the Fisher information and hence a smaller value of the relative error. However, this is obtained at the expense of the error enhancement in the momentum-based measurement. The squeezing effects are shown through the Wigner function (for its expression, see Appendix A) of the impurity state as in Fig. 4, where it is plotted against the phase space variables α_r and α_i . For higher dimensions, there is a less position squeezing effect and either of the measurements would result in the equivalent amount of error. For the 2D case, the separation of the error between position and momentum becomes lesser and both of them are always away from optimality, but within the same order of magnitude as the optimal measurement. For the 3D case the relative error for position and momentum measurements is equal, which is a reflection of the fact that both quadratures have the same temperature dependence. In this dimension the suboptimal measurements are not quite effective in extreme lows, but for $T \gtrsim 1$ nK they are within the same order of magnitude as the optimal measurement. Lastly, let us comment that as a result of thermalization at high enough temperatures ($T \gtrsim 10$ nK for 1D, $T \gtrsim 5$ nK for 2D, and $T \gtrsim 1$ nK for 3D) one has $\delta T(k)/T \approx \sqrt{2}\delta T_{\min}/T = \sqrt{2}$ for $k \in \{\hat{x}, \hat{p}\}$. This means with measuring position/momentum twice as many

times as the optimal measurement one can achieve the same target precision.

Perhaps the easiest way of performing the measurement of mean square displacement or momentum fluctuations could be done in the following scenario: Instead of looking at a single impurity, we can consider, say, 1000 to a few thousand of noninteracting impurities being polarized with cold Fermionic atoms. This idea contradicts in a sense the principal idea of the sample-probe interactions, where the probe size is significantly smaller than the sample, and that the sample is not directly measured. Still, with a condensate, say, 10^7 bosons, a few thousand probing, noninteracting Fermions will not make much difference. On the other hand, both their spatial and momentum density distributions are easily accessible experimentally: the former either through nondestructive light (refractive index) imaging or, more sophisticated, atomic microscopy, the latter through opening the trap for Fermions and looking at the momentum distribution in the time-of-flight measurement [63,64].

IV. CONCLUSION

Using an individual impurity as a temperature probe is crucial in nondemolition thermometry of cold gases; it has been studied theoretically in abstract models as well as more comprehensive ones in both fermionic and bosonic gases [3,7,23,24,65]. Recently, the idea was even put into experimental examination in the millikelvin thermometry of fermionic gases [37]. The results of the current work pave the path towards implementation of impurity-based thermometry in more versatile experimental setups of Bosonic gases in

different spacial dimensions $d = 1$, $d = 2$, and $d = 3$, for example [66–75].

Our results show that, for the temperature range $0.2 \leq T \leq 10$ nK, as one decreases the spatial dimension d the relative error reduces. Specifically, in the 3D scenario and for temperatures as small as $T \approx 0.2$ nK one can achieve the minimum relative error of 12.5% by $N = 100$ measurements. To achieve the same precision in the 1D case, one should perform more than $N = 400$ measurements. It must be noted that these are the fundamental bounds characterized by the quantum Cramér-Rao bound, they are in principle achievable, i.e., there exist physical measurements that can achieve such precisions. Nonetheless, experimental limitations will not allow for their realization. What is more doable are suboptimal Gaussian measurements, namely measuring position and momentum of the impurity.

In the 3D case and for $T \leq 0.5$ nK these measurements should be repeated an order of magnitude more than the optimal measurement in order to reach the same precision. For the 2D scenario one only requires few times more repetitions, while for the 1D scenario the position measurement is optimal. At higher temperatures, both position and momentum measurements perform very well and their relative error can be as good as the minimum error with twice as many measurements.

Apart from the experimental realization of our analysis, a possible future direction is the theoretical development of thermometry of bosonic gases by means of dynamical probes, i.e., measuring the probe before it reaches the steady state. This can be of more use in scenarios with long thermalization time. In such settings, the initial state of the impurity plays a crucial role in thermometry precision, and thus quantum resources at the initial state can be exploited for thermometry. Among these resources one can refer to the initial squeezing of the probe. It is well known that squeezing can improve metrology precision in phase estimation problems—i.e., when the parameter is encoded via a unitary dynamics [76–79]. While thermometry generally involves dissipative encoding of temperature, some recent works have shown that for short enough times squeezing can be indeed useful for thermometry [80]. Although this result was seen for Markovian dynamics, one can expect similar results when considering the BEC dynamics that we describe here, which are not necessarily Markovian.

In this work we mainly focused on local thermometry, where the parameter (temperature) is *a priori* known with a good precision, and one aims at estimating fluctuations around it. In some problems, however, one has a significant initial ignorance about the true parameter. These problems are termed *global* temperature estimation. For local parameter estimation problems the frequentist approach is the favorite, where the Cramér-Rao bound (CRB)—like those presented in this work—are valid even at single shot $N = 1$. When dealing with global schemes, the CRB is generally valid only at the asymptotic limit ($N \rightarrow \infty$). However, for the Gaussian measurements (position and momentum) that we use in this work, the Cramér-Rao bound is always valid, even for $N = 1$ and global schemes. This is so because when we perform these Gaussian measurements the probability of outcomes, i.e., $p(\mathbf{x}|\mathcal{P}, k)$, belongs to the family of Gaussian probability distributions, for which the Cramér-Rao bound saturates in single

shot—by means of a maximum likelihood estimation [81,82]. Beyond these measurements, e.g., for the optimal measurement, the best scheme for global thermometry remains the *Bayesian approach* that has been the focus of several recent works [18,83–87]. We leave this as an interesting problem for future exploration. Finally, taking the temperature of pure Bosonic gases, aligned with the recently proposed framework of [88], is an interesting problem that deserves further investigation.

ACKNOWLEDGMENTS

M.M.K. acknowledges support from Fundação para a Ciência e a Tecnologia (FCT-Portugal) through Grant No. PD/BD/114335/2016. H.T. acknowledges Fundação para a Ciência e a Tecnologia (FCT Portugal) through Contract No CEECIND/00401/2018, and the financial support through the Quantum Flagship Grant PhoQus (Grant No. 820392) of the European Union. M.A.G.M. acknowledges funding from the Spanish Ministry of Education and Vocational Training (MEFP) through the Beatriz Galindo program 2018 (BEAGAL18/00203). ICFO group acknowledges support from: ERC AdG NOQIA; Agencia Estatal de Investigación (R&D project CEX2019-000910-S, funded by MCIN/AEI/10.13039/501100011033, Plan National FIDEUA PID2019-106901GB-I00, FPI, QUANTERA MAQS PCI2019-111828-2, Proyectos de I+D+I “Retos Colaboración” QUSPIN RTC2019-007196-7); Fundació Cellex; Fundació Mir-Puig; Generalitat de Catalunya through the European Social Fund FEDER and CERCA program (AGAUR Grant No. 2017 SGR 134, QuantumCAT \ U16-011424, co-funded by ERDF Operational Program of Catalonia 2014-2020); EU Horizon 2020 FET-OPEN OPTologic (Grant No 899794); National Science Centre, Poland (Symfonia Grant No. 2016/20/W/ST4/00314); European Union’s Horizon 2020 research and innovation programme under the Marie-Skłodowska-Curie Grant Agreement No. 101029393 (STREDCH) and No. 847648 (“La Caixa” Junior Leaders fellowships ID100010434: LCF/BQ/PI19/11690013, LCF/BQ/PI20/11760031, LCF/BQ/PR20/11770012, LCF/BQ/PR21/11840013). M.M. acknowledges financial support from the Swiss National Science Foundation (NCCR SwissMAP). M.M.K. acknowledges Rey group at JILA for the hospitality and for providing the working conditions.

APPENDIX A: THERMAL STATISTIC OF THE IMPURITY

In order to calculate the thermal statistics of the impurity, we formally write the density operator of the impurity $\hat{\rho}_I$. Any physical state being represented by the density operator is bounded since its Hilbert Schmidt norm is finite. It is then possible to expand a boson mode state in the basis $\{\hat{D}^\dagger(\lambda) \forall \lambda \in \mathbb{C}, \lambda = \lambda_r + i\lambda_i\}$. Hence, one can write the state of the impurity as [89]

$$\hat{\rho}_I = \frac{1}{\pi^2} \int d^2\lambda \chi(\lambda, \lambda^*) \hat{D}^\dagger(\lambda). \quad (\text{A1})$$

Here $\hat{D}^\dagger(\lambda)$ is the conjugate transpose of the coherent displacement operator $\hat{D}(\lambda) = e^{\lambda\hat{a}^\dagger - \lambda^*\hat{a}}$ and $d^2\lambda = d\lambda_r d\lambda_i$ is the

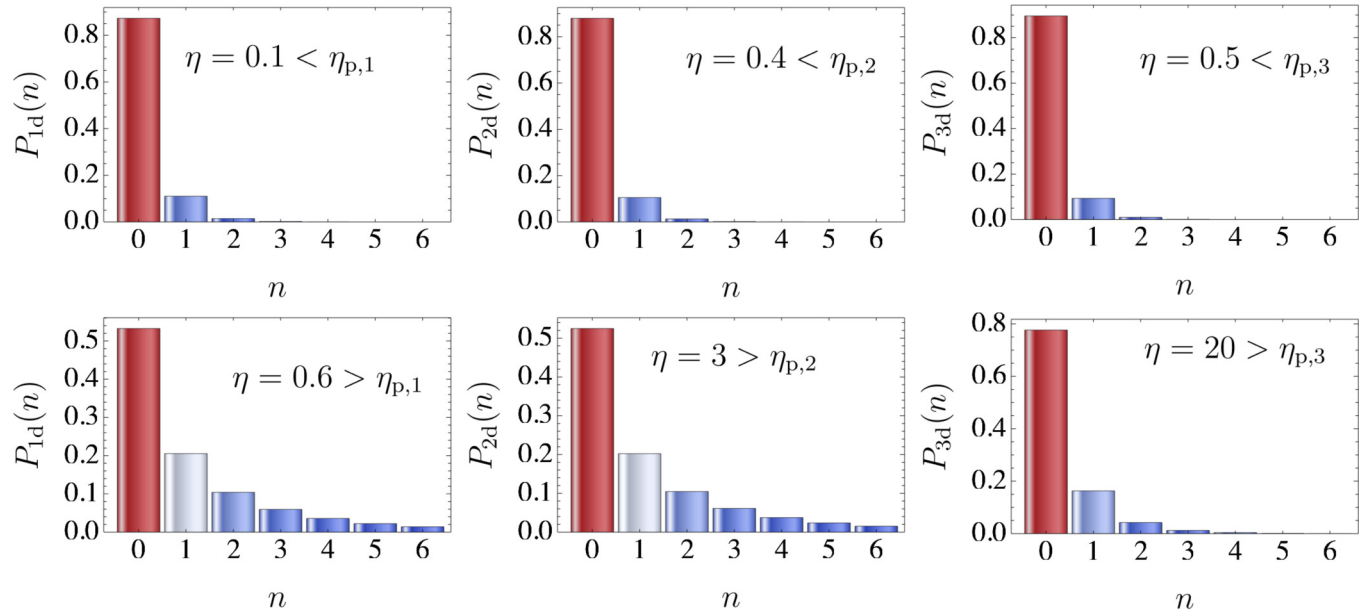


FIG. 5. Phonon number distribution of the impurity motion. Left, middle, and right columns represent the 1D, 2D, and 3D cases, respectively. The chosen couplings regimes and their values are shown in the inset of each of the figures. Rest of the parameters are the same as in Fig. 2.

measure for a two-dimensional integral corresponding to real part λ_r and imaginary part λ_i of the complex variable λ . For a canonical position \hat{x} and momentum \hat{p} variables associated with the harmonic oscillator, they can be expressed in terms of the quadrature $\hat{x} = (\hat{a} + \hat{a}^\dagger)/\sqrt{2}$ and $\hat{p} = i(\hat{a}^\dagger - \hat{a})/\sqrt{2}$, respectively. The commutation relation therefore reads $[\hat{x}, \hat{p}] = i$. Here \hat{a} (\hat{a}^\dagger) is the annihilation (creation) operator for the bosonic mode. In such coordinates $\alpha = (1/\sqrt{2})(\langle \hat{x} \rangle + i\langle \hat{p} \rangle)$. This reflects that the α_r and α_i are simply the scaled position and momentum expectation value and therefore a valid representation of the phase space. The symmetric ordered characteristic function $\chi(\beta, \beta^*)$ is the expectation value of the Weyl operator, given by $\chi(\beta, \beta^*) = \text{Tr}[\hat{\rho}_1 \hat{D}(\beta)]$. If the dynamics is Gaussian, the quantum characteristic function is fully captured by the covariance matrix by the expression $\chi(\beta, \beta^*) = e^{-(1/2)\mathbf{x}\sigma\mathbf{x}^T}$. Here σ is the covariance matrix associated with the mode and $\mathbf{x} = (\beta_i, \beta_r)$ are the phase space variables [90]. The Wigner quasiprobability distribution function $W(\alpha, \alpha^*)$ is the two-dimensional complex Fourier transform of the characteristic function such that

$$W(\alpha, \alpha^*) = \frac{1}{\pi^2} \int d^2\beta \chi(\beta, \beta^*) e^{-(\beta\alpha^* - \beta^*\alpha)}. \quad (\text{A2})$$

In addition, the phonon number statistics, that is, the probability of finding n phonon in the mode, is connected to the density operator by the expression $P(n) = \langle n | \hat{\rho}_1 | n \rangle$. This can be calculated via the matrix elements of the displacement operator being evaluated in the Fock basis and given by the expression [91]

$$\langle n | \hat{D}(\alpha) | m \rangle = \sqrt{\frac{m!}{n!}} e^{-|\alpha|^2/2} (\alpha)^{n-m} \mathcal{L}_m^{n-m}[|\alpha|^2], \quad n \geq m, \quad (\text{A3})$$

where $\mathcal{L}_m^{n-m}[\cdot]$ are the generalized Laguerre polynomials. In the present case we are mainly interested in the diagonal en-

tries, therefore we have $m = n$. We plot the impurity phonon number distribution both for $\eta < \eta_{p,d}$ and $\eta > \eta_{p,d}$ for each dimension in Fig. 5. For the $\eta < \eta_{p,d}$ thermal statistics of the impurity are almost fully contributed by the ground state while for $\eta > \eta_{p,d}$, higher order Fock states contribute significantly in the construction of the thermal phonon statistics.

APPENDIX B: RELATIVE ERROR FOR EXTENDED TEMPERATURE RANGE DOWN TO 50 pK

In this Appendix we show the relative error for the low temperature domain down to 50 pK. This reflects how much the relative error enhances as we move to lower values of the temperature. As such, the cases based on optimal measurements are shown in Fig. 6. Here the relative error of the 3D case starts deviating from the thermal profile at temperature

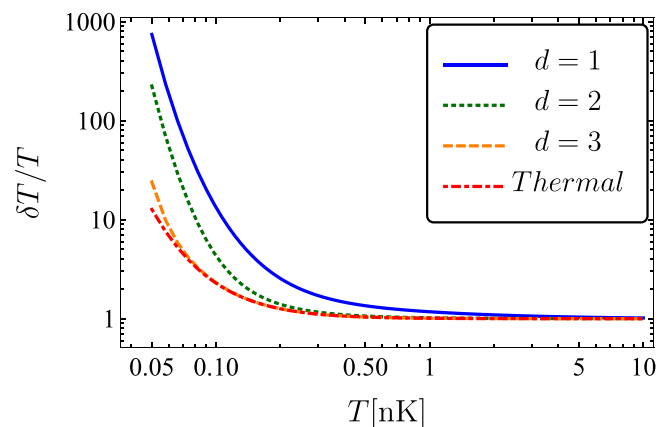


FIG. 6. Same as in Fig. 3, only the temperature domain has been extended within the interval $0.05 \leq T \leq 10$ nK.

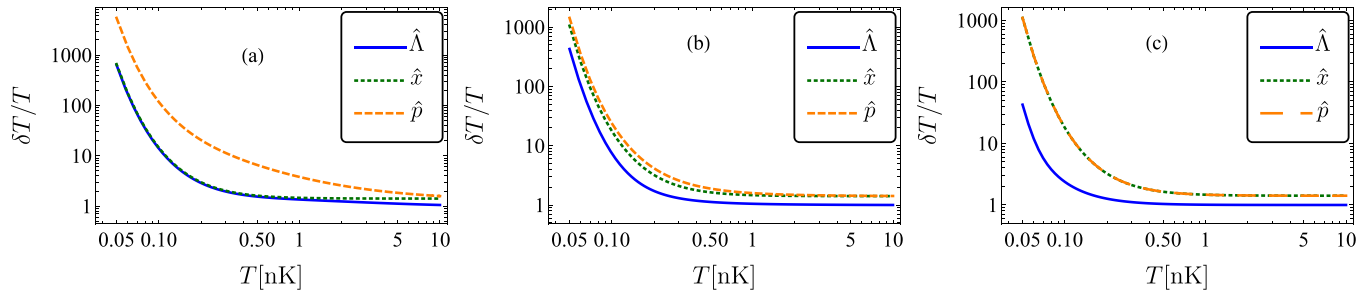


FIG. 7. Same as in the upper panel of Fig. 4 of the main text, however, temperature domain has been extended within the interval $0.05 \leq T \leq 10$ nK.

below $T \simeq 60$ pK. Moreover, the relative errors based on the suboptimal measurements are shown in Figs. 7(a)–7(c).

APPENDIX C: SPECTRAL FUNCTION

The Bogoliubov bosonic environment is characterized through the self-correlation function

$$\underline{\underline{C}}(\tau) = \sum_{\mathbf{k} \neq 0} \hbar \underline{\underline{g}}_{\mathbf{k}} \langle \pi_{\mathbf{k}}(\tau) \pi_{\mathbf{k}}(0) \rangle, \quad (\text{C1})$$

with $\underline{\underline{g}}_{\mathbf{k}} = g_{\mathbf{k}} g_{\mathbf{k}}^T$ representing the coupling tensor in a given dimension d . The environment at the finite temperature T follows the Bose-Einstein statistics. Therefore, the mean number of bosons in each of the bath modes is given by

$$\langle b_{\mathbf{k}}^\dagger b_{\mathbf{k}} \rangle = \frac{1}{\exp(\hbar \omega_{\mathbf{k}} / k_B T) - 1}. \quad (\text{C2})$$

In order to calculate the correlation, we invoke the expression for the dimensionless momenta and make use of Eqs. (C2) and (C1) which results in

$$\begin{aligned} \underline{\underline{C}}(\tau) &= \sum_{\mathbf{k} \neq 0} \hbar \underline{\underline{g}}_{\mathbf{k}} \left[\coth\left(\frac{\hbar \omega_{\mathbf{k}}}{2k_B T}\right) \cos(\omega_{\mathbf{k}} \tau) - i \sin(\omega_{\mathbf{k}} \tau) \right] \\ &\equiv \underline{\underline{v}}(\tau) - i \underline{\underline{\lambda}}(\tau), \end{aligned} \quad (\text{C3})$$

where the real and imaginary part of the self-correlation function are given by

$$\underline{\underline{v}}(\tau) = \int_0^\infty \underline{\underline{J}}(\omega) \coth\left(\frac{\hbar \omega}{2k_B T}\right) \cos(\omega \tau) d\omega, \quad (\text{C4})$$

$$\underline{\underline{\lambda}}(\tau) = \int_0^\infty \underline{\underline{J}}(\omega) \sin(\omega \tau) d\omega = -m_1 \dot{\underline{\underline{\Gamma}}}(\tau). \quad (\text{C5})$$

Moreover, the damping kernel $\underline{\underline{\Gamma}}(t)$ can be obtained from the expression

$$\underline{\underline{\Gamma}}(t) = (1/m_1) \int_0^\infty d\omega (1/\omega) \underline{\underline{J}}(\omega) \cos(\omega t). \quad (\text{C6})$$

In the above expressions we have introduced the spectral density $\underline{\underline{J}}(\omega)$, which fully characterizes the effects of the bath on the system. This information is contained in the coupling strengths of the various modes of the bath with the system. The spectral density is defined as

$$\underline{\underline{J}}(\omega) = \sum_{\mathbf{k} \neq 0} \hbar \underline{\underline{g}}_{\mathbf{k}} \delta(\omega - \omega_{\mathbf{k}}). \quad (\text{C7})$$

The expression for the spectral density tensor for a given dimension has been formulated in Ref. [51]. This has been shown to take the form

$$\underline{\underline{J}}_d(\omega) = d^{-1} [\underline{\underline{J}}_d(\omega)] \underline{\underline{I}}_{d \times d}, \quad (\text{C8})$$

where $\underline{\underline{I}}_{d \times d}$ is the identity matrix and the scalar spectral function $\underline{\underline{J}}_d(\omega)$ in dimension d is given by

$$\begin{aligned} \underline{\underline{J}}_d(\omega) &= \left(\frac{S_d (\sqrt{2})^d (\eta_d)^2 (\Lambda_d)^{d+2}}{(2\pi)^d} \right) \\ &\times \left(\frac{\left[\left(\frac{m_B}{[g_{B,d}]^{d+2}} \right) \left(\sqrt{\frac{\omega^2}{(\Lambda_d)^2} + 1} - 1 \right) \right]^{\frac{d+2}{2}}}{\left(\sqrt{\frac{\omega^2}{(\Lambda_d)^2} + 1} \right)} \right). \end{aligned} \quad (\text{C9})$$

Here for $d = 1, 2$, and 3 we have $S_1 = 2$, $S_2 = 2\pi$, and $S_3 = 4\pi$, respectively. Moreover, we have introduced the characteristic frequency $\Lambda_d = (g_{B,d} n_{0,d}) / \hbar$. We also write the impurity-boson coupling in the units of the boson-boson coupling as $\eta_d = (g_{IB,d} / g_{B,d})$, and Λ_d naturally appears as the characteristic cut-off frequency. Within the low frequency part given by $\omega \lesssim \Lambda_d$, and together with the introduction of the cutoff, the spectral function takes the form as presented in Eq. (8) of the main text [51].

[1] M. Mehboudi, A. Sanpera, and L. A. Correa, Thermometry in the quantum regime: Recent theoretical progress, *J. Phys. A: Math. Theor.* **52**, 303001 (2019).

[2] A. De Pasquale and T. M. Stace, Quantum thermometry, in *Thermodynamics in the Quantum Regime* (Springer, New York, 2018), pp. 503–527.

[3] M. Mehboudi, A. Lampo, C. Charalambous, L. A. Correa, M. Á. García-March, and M. Lewenstein, Using Polarons for sub-nK Quantum Nondemolition Thermometry in a Bose-Einstein Condensate, *Phys. Rev. Lett.* **122**, 030403 (2019).

[4] S. Razavian, C. Benedetti, M. Bina, Y. Akbari-Kourbolagh, and M. G. A. Paris, Quantum thermometry by

- single-qubit dephasing, *Eur. Phys. J. Plus* **134**, 284 (2019).
- [5] S. Seah, S. Nimmrichter, D. Grimmer, J. P. Santos, V. Scarani, and G. T. Landi, Collisional Quantum Thermometry, *Phys. Rev. Lett.* **123**, 180602 (2019).
- [6] L. A. Correa, M. Mehboudi, G. Adesso, and A. Sanpera, Individual Quantum Probes for Optimal Thermometry, *Phys. Rev. Lett.* **114**, 220405 (2015).
- [7] M. T. Mitchison, T. Fogarty, G. Guarnieri, S. Campbell, T. Busch, and J. Goold, *In Situ* Thermometry of a Cold Fermi Gas via Dephasing Impurities, *Phys. Rev. Lett.* **125**, 080402 (2020).
- [8] A. De Pasquale, D. Rossini, R. Fazio, and V. Giovannetti, Local quantum thermal susceptibility, *Nat. Commun.* **7**, 12782 (2016).
- [9] M. G. A. Paris, Achieving the Landau bound to precision of quantum thermometry in systems with vanishing gap, *J. Phys. A: Math. Theor.* **49**, 03LT02 (2016).
- [10] K. V. Hovhannisyán and L. A. Correa, Measuring the temperature of cold many-body quantum systems, *Phys. Rev. B* **98**, 045101 (2018).
- [11] M. Mehboudi, M. Moreno-Cardoner, G. De Chiara, and A. Sanpera, Thermometry precision in strongly correlated ultracold lattice gases, *New J. Phys.* **17**, 055020 (2015).
- [12] S. S. Mirkhalaf, D. Benedicto Orenes, M. W. Mitchell, and E. Witkowska, Criticality-enhanced quantum sensing in ferromagnetic Bose-Einstein condensates: Role of readout measurement and detection noise, *Phys. Rev. A* **103**, 023317 (2021).
- [13] P. P. Hofer, J. B. Brask, M. Perarnau-Llobet, and N. Brunner, Quantum Thermal Machine as a Thermometer, *Phys. Rev. Lett.* **119**, 090603 (2017).
- [14] G. A. Paz-Silva, L. M. Norris, and L. Viola, Multiqubit spectroscopy of Gaussian quantum noise, *Phys. Rev. A* **95**, 022121 (2017).
- [15] S. Campbell, M. Mehboudi, G. De Chiara, and M. Paternostro, Global and local thermometry schemes in coupled quantum systems, *New J. Phys.* **19**, 103003 (2017).
- [16] W.-K. Mok, K. Bharti, L.-C. Kwek, and A. Bayat, Optimal probes for global quantum thermometry, *Commun. Phys.* **4**, 62 (2021).
- [17] C. L. Latune, I. Sinayskiy, and F. Petruccione, Collective heat capacity for quantum thermometry and quantum engine enhancements, *New J. Phys.* **22**, 083049 (2020).
- [18] J. Rubio, J. Anders, and L. A. Correa, Global Quantum Thermometry, *Phys. Rev. Lett.* **127**, 190402 (2021).
- [19] P. P. Potts, J. B. Brask, and N. Brunner, Fundamental limits on low-temperature quantum thermometry with finite resolution, *Quantum* **3**, 161 (2019).
- [20] M. R. Jørgensen, P. P. Potts, M. G. A. Paris, and J. B. Brask, Tight bound on finite-resolution quantum thermometry at low temperatures, *Phys. Rev. Research* **2**, 033394 (2020).
- [21] H.-P. Breuer and F. Petruccione, *The Theory of Open Quantum Systems* (Oxford University Press on Demand, 2002).
- [22] U. Weiss, *Quantum Dissipative Systems* (World Scientific, Singapore, 2012), Vol. 13.
- [23] L. A. Correa, M. Perarnau-Llobet, K. V. Hovhannisyán, S. Hernández-Santana, M. Mehboudi, and A. Sanpera, Enhancement of low-temperature thermometry by strong coupling, *Phys. Rev. A* **96**, 062103 (2017).
- [24] G. Planella, M. F. B. Cenni, A. Acín, and M. Mehboudi, Bath-induced correlations lead to sub-shot-noise thermometry precision, *Phys. Rev. Lett.* **128**, 040502 (2022).
- [25] A. L. Gaunt, T. F. Schmidutz, I. Gotlibovych, R. P. Smith, and Z. Hadzibabic, Bose-Einstein Condensation of Atoms in a Uniform Potential, *Phys. Rev. Lett.* **110**, 200406 (2013).
- [26] A. Jaouadi, N. Gaaloul, B. Viaris de Lesegno, M. Telmini, L. Pruvost, and E. Charron, Bose-Einstein condensation in dark power-law laser traps, *Phys. Rev. A* **82**, 023613 (2010).
- [27] A. Kaplan, N. Friedman, and N. Davidson, Optimized single-beam dark optical trap, *J. Opt. Soc. Am. B* **19**, 1233 (2002).
- [28] I. Gotlibovych, T. F. Schmidutz, A. L. Gaunt, N. Navon, R. P. Smith, and Z. Hadzibabic, Observing properties of an interacting homogeneous Bose-Einstein condensate: Heisenberg-limited momentum spread, interaction energy, and free-expansion dynamics, *Phys. Rev. A* **89**, 061604(R) (2014).
- [29] T. F. Schmidutz, I. Gotlibovych, A. L. Gaunt, R. P. Smith, N. Navon, and Z. Hadzibabic, Quantum Joule-Thomson Effect in a Saturated Homogeneous Bose Gas, *Phys. Rev. Lett.* **112**, 040403 (2014).
- [30] L. Corman, L. Chomaz, T. Bienaimé, R. Desbuquois, C. Weitenberg, S. Nascimbène, J. Dalibard, and J. Beugnon, Quench-Induced Supercurrents in an Annular Bose Gas, *Phys. Rev. Lett.* **113**, 135302 (2014).
- [31] L. Chomaz, L. Corman, T. Bienaimé, R. Desbuquois, C. Weitenberg, S. Nascimbène, J. Beugnon, and J. Dalibard, Emergence of coherence via transverse condensation in a uniform quasi-two-dimensional Bose gas, *Nat. Commun.* **6**, 6162 (2015).
- [32] N. Navon, A. L. Gaunt, R. P. Smith, and Z. Hadzibabic, Critical dynamics of spontaneous symmetry breaking in a homogeneous Bose gas, *Science* **347**, 167 (2015).
- [33] J. Beugnon and N. Navon, Exploring the Kibble-Zurek mechanism with homogeneous Bose gases, *J. Phys. B: At., Mol. Opt. Phys.* **50**, 022002 (2017).
- [34] R. Lopes, C. Eigen, N. Navon, D. Clément, R. P. Smith, and Z. Hadzibabic, Quantum Depletion of a Homogeneous Bose-Einstein Condensate, *Phys. Rev. Lett.* **119**, 190404 (2017).
- [35] R. Lopes, C. Eigen, A. Barker, K. G. H. Viebahn, M. Robert-de Saint-Vincent, N. Navon, Z. Hadzibabic, and R. P. Smith, Quasiparticle Energy in a Strongly Interacting Homogeneous Bose-Einstein Condensate, *Phys. Rev. Lett.* **118**, 210401 (2017).
- [36] G. Gauthier, M. T. Reeves, X. Yu, A. S. Bradley, M. A. Baker, T. A. Bell, H. Rubinsztein-Dunlop, M. J. Davis, and T. W. Neely, Giant vortex clusters in a two-dimensional quantum fluid, *Science* **364**, 1264 (2019).
- [37] Q. Bouton, J. Nettersheim, D. Adam, F. Schmidt, D. Mayer, T. Lausch, E. Tiemann, and A. Widera, Single-Atom Quantum Probes for Ultracold Gases Boosted by Nonequilibrium Spin Dynamics, *Phys. Rev. X* **10**, 011018 (2020).
- [38] J. D. Reppy, B. C. Crooker, B. Hebral, A. D. Corwin, J. He, and G. M. Zassenhaus, Density Dependence of the Transition Temperature in a Homogeneous Bose-Einstein Condensate, *Phys. Rev. Lett.* **84**, 2060 (2000).
- [39] P. Arnold and G. Moore, BEC Transition Temperature of a Dilute Homogeneous Imperfect Bose Gas, *Phys. Rev. Lett.* **87**, 120401 (2001).
- [40] V. A. Kashurnikov, N. V. Prokof'ev, and B. V. Svistunov, Critical Temperature Shift in Weakly Interacting Bose Gas, *Phys. Rev. Lett.* **87**, 120402 (2001).

- [41] H. Kleinert, Five-loop critical temperature shift in weakly interacting homogeneous Bose–Einstein condensate, *Mod. Phys. Lett. B* **17**, 1011 (2003).
- [42] B. Kastening, Bose-Einstein condensation temperature of a homogenous weakly interacting Bose gas in variational perturbation theory through seven loops, *Phys. Rev. A* **69**, 043613 (2004).
- [43] H. Kleinert, S. Schmidt, and A. Pelster, Quantum phase diagram for homogeneous Bose-Einstein condensate, *Annal. Phys.* **14**, 214 (2005).
- [44] V. I. Yukalov and E. P. Yukalova, Normal and anomalous averages for systems with Bose-Einstein condensate, *Laser Phys. Lett.* **2**, 506 (2005).
- [45] B. Opanchuk, R. Polkinghorne, O. Fialko, J. Brand, and P. D. Drummond, Quantum simulations of the early universe, *Annal. Phys.* **525**, 866 (2013).
- [46] O. Fialko, B. Opanchuk, A. I. Sidorov, P. D. Drummond, and J. Brand, Fate of the false vacuum: Towards realization with ultra-cold atoms, *Europhys. Lett.* **110**, 56001 (2015).
- [47] K. L. Ng, B. Opanchuk, M. Thenabadu, M. Reid, and P. D. Drummond, Fate of the false vacuum: Finite temperature, entropy, and topological phase in quantum simulations of the early universe, *PRX Quantum* **2**, 010350 (2021).
- [48] M. Ahmadi, D. E. Bruschi, C. Sabín, G. Adesso, and I. Fuentes, Relativistic quantum metrology: Exploiting relativity to improve quantum measurement technologies, *Sci. Rep.* **4**, 4996 (2014).
- [49] A. Lampo, S. H. Lim, M. Á. García-March, and M. Lewenstein, Bose polaron as an instance of quantum Brownian motion, *Quantum* **1**, 30 (2017).
- [50] A. Lampo, C. Charalambous, M. Á. García-March, and M. Lewenstein, Non-Markovian polaron dynamics in a trapped Bose-Einstein condensate, *Phys. Rev. A* **98**, 063630 (2018).
- [51] M. M. Khan, H. Terças, J. T. Mendonça, J. Wehr, C. Charalambous, M. Lewenstein, and M. A. Garcia-March, Quantum dynamics of a Bose polaron in a d -dimensional Bose-Einstein condensate, *Phys. Rev. A* **103**, 023303 (2021).
- [52] G. E. Astrakharchik and L. P. Pitaevskii, Motion of a heavy impurity through a Bose-Einstein condensate, *Phys. Rev. A* **70**, 013608 (2004).
- [53] D. K. Efimkin, J. Hofmann, and V. Galitski, Non-Markovian Quantum Friction of Bright Solitons in Superfluids, *Phys. Rev. Lett.* **116**, 225301 (2016).
- [54] J. Eisert, S. Scheel, and M. B. Plenio, Distilling Gaussian States with Gaussian Operations is Impossible, *Phys. Rev. Lett.* **89**, 137903 (2002).
- [55] S. L. Braunstein and C. M. Caves, Statistical Distance and the Geometry of Quantum States, *Phys. Rev. Lett.* **72**, 3439 (1994).
- [56] M. G. A. PARIS, Quantum estimation for quantum technology, *Int. J. Quantum. Inform.* **07**, 125 (2009).
- [57] A. Monras, Phase space formalism for quantum estimation of Gaussian states, [arXiv:1303.3682](https://arxiv.org/abs/1303.3682).
- [58] Z. Jiang, Quantum fisher information for states in exponential form, *Phys. Rev. A* **89**, 032128 (2014).
- [59] O. Pinel, P. Jian, N. Treps, C. Fabre, and D. Braun, Quantum parameter estimation using general single-mode Gaussian states, *Phys. Rev. A* **88**, 040102(R) (2013).
- [60] M. G. Genoni, O. S. Duarte, and A. Serafini, Unravelling the noise: The discrimination of wave function collapse models under time-continuous measurements, *New J. Phys.* **18**, 103040 (2016).
- [61] M. F. B. Cenni, L. Lami, A. Acin, and M. Mehboudi, Thermometry of Gaussian quantum systems using Gaussian measurements, [arXiv:2110.02098](https://arxiv.org/abs/2110.02098).
- [62] O. Romero-Isart, A. C. Pflanzer, F. Blaser, R. Kaltenbaek, N. Kiesel, M. Aspelmeyer, and J. I. Cirac, Large Quantum Superpositions and Interference of Massive Nanometer-Sized Objects, *Phys. Rev. Lett.* **107**, 020405 (2011).
- [63] J. E. Lye, B. D. Cuthbertson, H.-A. Bachor, and J. D. Close, Phase modulation spectroscopy: A non-destructive probe of Bose-Einstein condensates, *J. Opt. B: Quantum Semiclassical Opt.* **1**, 402 (1999).
- [64] M. R. Andrews, M.-O. Mewes, N. J. van Druten, D. S. Durfee, D. M. Kurn, and W. Ketterle, Direct, nondestructive observation of a Bose condensate, *Science* **273**, 84 (1996).
- [65] R. Onofrio, Physics of our days: Cooling and thermometry of atomic Fermi gases, *Phys. Usp.* **59**, 1129 (2016).
- [66] J. Catani, G. Lamporesi, D. Naik, M. Gring, M. Inguscio, F. Minardi, A. Kantian, and T. Giamarchi, Quantum dynamics of impurities in a one-dimensional Bose gas, *Phys. Rev. A* **85**, 023623 (2012).
- [67] N. Spethmann, F. Kindermann, S. John, C. Weber, D. Meschede, and A. Widera, Dynamics of Single Neutral Impurity Atoms Immersed in an Ultracold Gas, *Phys. Rev. Lett.* **109**, 235301 (2012).
- [68] M. Hohmann, F. Kindermann, B. Gänger, T. Lausch, D. Mayer, F. Schmidt, and A. Widera, Neutral impurities in a Bose-Einstein condensate for simulation of the Fröhlich-polaron, *EPJ Quantum Technol.* **2**, 23 (2015).
- [69] F. Schmidt, D. Mayer, Q. Bouton, D. Adam, T. Lausch, N. Spethmann, and A. Widera, Quantum Spin Dynamics of Individual Neutral Impurities Coupled to a Bose-Einstein Condensate, *Phys. Rev. Lett.* **121**, 130403 (2018).
- [70] T. Rentrop, A. Trautmann, F. A. Olivares, F. Jendrzejewski, A. Komnik, and M. K. Oberthaler, Observation of the Phononic Lamb Shift with a Synthetic Vacuum, *Phys. Rev. X* **6**, 041041 (2016).
- [71] R. Scelle, T. Rentrop, A. Trautmann, T. Schuster, and M. K. Oberthaler, Motional Coherence of Fermions Immersed in a Bose Gas, *Phys. Rev. Lett.* **111**, 070401 (2013).
- [72] C. Zipkes, S. Palzer, C. Sias, and M. Köhl, A trapped single ion inside a Bose–Einstein condensate, *Nature (London)* **464**, 388 (2010).
- [73] N. B. Jørgensen, L. Wacker, K. T. Skalmstang, M. M. Parish, J. Levinsen, R. S. Christensen, G. M. Bruun, and J. J. Arlt, Observation of Attractive and Repulsive Polarons in a Bose-Einstein Condensate, *Phys. Rev. Lett.* **117**, 055302 (2016).
- [74] M.-G. Hu, M. J. Van de Graaff, D. Kedar, J. P. Corson, E. A. Cornell, and D. S. Jin, Bose Polarons in the Strongly Interacting Regime, *Phys. Rev. Lett.* **117**, 055301 (2016).
- [75] Z. Z. Yan, Y. Ni, C. Robens, and M. W. Zwierlein, Bose polarons near quantum criticality, *Science* **368**, 190 (2020).
- [76] C. M. Caves, Quantum-mechanical noise in an interferometer, *Phys. Rev. D* **23**, 1693 (1981).
- [77] L. Pezzé and A. Smerzi, Mach-Zehnder Interferometry at the Heisenberg Limit with Coherent and Squeezed-Vacuum Light, *Phys. Rev. Lett.* **100**, 073601 (2008).

- [78] R. Demkowicz-Dobrzański, M. Jarzyna, and J. Kołodyński, *Chapter Four—Quantum Limits in Optical Interferometry* (Elsevier, Amsterdam, 2015), pp. 345–435.
- [79] C. Gross, Spin squeezing, entanglement and quantum metrology with Bose-Einstein condensates, *J. Phys. B: At., Mol. Opt. Phys.* **45**, 103001 (2012).
- [80] L. Mancino, M. G. Genoni, M. Barbieri, and M. Paternostro, Nonequilibrium readiness and precision of Gaussian quantum thermometers, *Phys. Rev. Research* **2**, 033498 (2020).
- [81] S. M. Kay, *Fundamentals of Statistical Signal Processing: Estimation Theory* (Prentice-Hall, Englewood Cliffs, NJ, 1993).
- [82] J. Kolodnyski, Precision bounds in noisy quantum metrology, [arXiv:1409.0535](https://arxiv.org/abs/1409.0535).
- [83] M. R. Jørgensen, J. Kołodyński, M. Mehboudi, M. Perarnau-Llobet, and J. B. Brask, Bayesian quantum thermometry based on thermodynamic length, *Phys. Rev. A* **105**, 042601 (2022).
- [84] J. Boeyens, S. Seah, and S. Nimmrichter, Uninformed Bayesian quantum thermometry, *Phys. Rev. A* **104**, 052214 (2021).
- [85] M. Mehboudi, M. R. Jørgensen, S. Seah, J. B. Brask, J. Kołodyński, and M. Perarnau-Llobet, Fundamental Limits in Bayesian Thermometry and Attainability via Adaptive Strategies, *Phys. Rev. Lett.* **128**, 130502 (2022).
- [86] G. O. Alves and G. T. Landi, Bayesian estimation for collisional thermometry, *Phys. Rev. A* **105**, 012212 (2022).
- [87] J. Rubio, Quantum scale estimation, [arXiv:2111.11921](https://arxiv.org/abs/2111.11921).
- [88] M. T. Mitchison, A. Purkayastha, M. Brenes, A. Silva, and J. Goold, Taking the temperature of a pure quantum state, *Phys. Rev. A* **105**, L030201 (2022).
- [89] K. E. Cahill and R. J. Glauber, Density operators and quasiprobability distributions, *Phys. Rev.* **177**, 1882 (1969).
- [90] L.-M. Duan, G. Giedke, J. I. Cirac, and P. Zoller, Inseparability Criterion for Continuous Variable Systems, *Phys. Rev. Lett.* **84**, 2722 (2000).
- [91] F. A. M. de Oliveira, M. S. Kim, P. L. Knight, and V. Buzek, Properties of displaced number states, *Phys. Rev. A* **41**, 2645 (1990).